



# Modification of temporal pattern sensitivity for inputs from medial entorhinal cortex by lateral inputs in hippocampal granule cells

Naoki Nakajima<sup>1</sup> · Tadanobu Kamijo<sup>2</sup> · Hirofumi Hayakawa<sup>1</sup> · Eriko Sugisaki<sup>3</sup> · Takeshi Aihara<sup>1,3</sup>

Received: 1 November 2022 / Revised: 8 March 2023 / Accepted: 23 March 2023 / Published online: 13 April 2023  
© The Author(s), under exclusive licence to Springer Nature B.V. 2023

## Abstract

The medial dendrites (MDs) of granule cells (GCs) receive spatial information through the medial entorhinal cortex (MEC) from the entorhinal cortex in the rat hippocampus while the distal dendrites (DDs) of GCs receive non-spatial information (sensory inputs) through the lateral entorhinal cortex (LEC). However, it is unclear how information processing through the two pathways is managed in GCs. In this study, we investigated associative information processing between two independent inputs to MDs and DDs. First, in physiological experiments, to compare response characteristics between MDs and DDs, electrical stimuli comprising five pulses were applied to the MPP or LPP in rat hippocampal slices. These stimuli transiently decreased the excitatory postsynaptic potentials (EPSPs) of successive input pulses to MDs, whereas EPSPs to DDs showed sustained responses. Next, in computational experiments using a local network model obtained by fitting of the physiological experimental data, we compared associative information processing between DDs and MDs. The results showed that the temporal pattern sensitivity for burst inputs to MDs depended on the frequency of the random pulse inputs applied to DDs. On the other hand, with lateral inhibition to GCs from interneurons, the temporal pattern sensitivity for burst inputs to MDs was enhanced or tuned up according to the frequency of the random pulse inputs to the other cells. Thus, our results suggest that the temporal pattern sensitivity of spatial information depends on the non-spatial inputs to GCs.

**Keywords** Hippocampal granule cell · Spatial information · Modification · Interneuron · Associative information processing

## Introduction

The dentate gyrus (DG) is located at the entrance to the hippocampus and receives input from the entorhinal cortex (EC) through two pathways (Burwell and Amaral 1998). One, the lateral perforant path (LPP), originates in the lateral entorhinal cortex (LEC), while the other, the medial perforant path (MPP), originates in the medial entorhinal cortex (MEC); they terminate in the outer and middle

molecular layers of the DG, respectively (Young et al. 1997; Nishimura-Akiyoshi et al. 2007). LEC neurons respond to non-spatial information [such as objects (Deshmukh and Knierim 2011) and odor (Young et al. 1997; Xu and Wilson 2012)], and their activity is less regular than that of MEC neurons (Deshmukh et al. 2010). In contrast, MEC neurons emit brief bursts at  $\theta$  intervals during explorative behavior and sleep (Alonso and García-Austt 1987; Jeewajee et al. 2008; Deshmukh et al. 2010; Sullivan et al. 2014). Non-spatial and spatial information is considered to be delivered to granule cells (GCs) in the DG from the LEC and MEC, respectively. In addition, feed-forward inhibitory inputs from the LPP and MPP from basket cells are input to the proximal dendrites or cell bodies of GCs. It was previously reported that the feed-forward inhibition induced by the MPP to MDs was smaller than that induced by the LPP to DDs (Ceranik et al. 1997; Booker and Vida 2018). Using rat hippocampal slices,

✉ Takeshi Aihara  
aihara@eng.tamagawa.ac.jp

<sup>1</sup> Graduated School of Engineering, Tamagawa University, Tokyo, Japan

<sup>2</sup> Graduate School of Medicine, University of the Ryukyus, Okinawa, Japan

<sup>3</sup> Brain Science Institute, Tamagawa University, Tokyo, Japan

paired stimuli were also determined to cause paired-pulse facilitation in the LPP and paired-pulse depression in the MPP (Colino and Malenka 1993). This indicates a difference in the presynaptic properties of inputs to GCs (McNaughton 1980; Colino and Malenka 1993; Petersen et al. 2013).

“Place cells”, which are activated only when a specific location is passed, are active in  $\theta$  rhythm (about 8 Hz) (O’Keefe and Recce 1993; Skaggs et al. 1996) while local field potentials in the LEC exhibit strong oscillations in the 20–40-Hz band during the cue sampling period (Igarashi et al. 2014). Thus, medial dendrites (MDs) receive  $\theta$ -burst input from the MEC while distal dendrites (DDs) receive 20–40-Hz pulse input from the LEC. Our previous study showed how the 10- and 20-Hz LPP inputs are integrated in GCs with the 8-Hz  $\theta$  bursts from the MPP (Hayakawa et al. 2015). However, the 20–40-Hz input from the LPP has not been discussed for this frequency range. This suggests that these two types of information may interact in GCs at different input frequencies. In addition, the existence and role of lateral inhibition in the DG in terms of memory have recently been studied (Sun et al. 2020; Tuncdemir et al. 2022). Moreover, it has been reported that lateral inhibition in the DG is more abundant than recurrent inhibition (Espinoza et al. 2018). However, it is not known how the  $\theta$  rhythm input of the MPP and the 20–40 Hz inputs of the LPP interact with inhibitory inputs in GCs.

In the present study, we first performed electrophysiological experiments using rat hippocampal slices to investigate the frequency responses of MDs and DDs. In the experiments, five successive electrical pulses were applied to the MPP and LPP, and extracellular field excitatory postsynaptic potentials (fEPSPs) were measured. MDs and DDs showed sustained and transient responses, respectively. Next, we performed computer simulation experiments using a GC model fixed by parameter fitting from the physiological data. In the simulation, we developed a dynamic synapse and multi-compartment model of GCs. To investigate the associative effects of MD and DD inputs on the information processing of GCs, we simultaneously applied  $\theta$ -burst and 10–40-Hz random pulse inputs. Furthermore, we built another network with lateral inhibition in which GCs receiving inputs to DDs from the LPP inhibited GCs receiving inputs to MDs from the MPP. In the network, 10–40-Hz random pulses were applied to DDs and  $\theta$ -burst inputs were applied to MDs. In the network with lateral inhibition, the temporal pattern sensitivity for burst input to MDs was enhanced according to the frequency of the random pulse inputs to DDs. Thus, our results suggest that the information processing of GCs for temporal pattern inputs depends on the non-spatial information in the DG network.

## Materials and methods

### Slice preparation

Transverse hippocampal slices were prepared from 3–4-week-old Wistar rats. The brain was removed from rats anesthetized using isoflurane. Transverse hippocampal slices (400  $\mu$ m) were made using a Microslicer (DTK-1000, Dosaka EM Corp.) in cold artificial cerebrospinal fluid (ACSF) containing (in mM) 124 NaCl, 3 KCl, 10 glucose, 1.25  $\text{NaH}_2\text{PO}_4$ , 22  $\text{NaHCO}_3$ , 2  $\text{MgSO}_4$ , and 2.5  $\text{CaCl}_2$  (pH 7.3 when bubbled with 95%  $\text{O}_2$  and 5%  $\text{CO}_2$ ). Experiments were then performed after the brain slices were stored at room temperature for 1 hour. All procedures were approved by the Tamagawa University Animal Care and Use Committee.

### Recordings and electrophysiological experiments

Two monopolar glass electrodes were placed on the outer molecular layer and middle molecular layer in the DG to record fEPSPs evoked by pulse trains (Fig. 1) because the LPP and MPP project from the EC to the outer molecular layer and middle molecular layer in the DG, respectively (McNaughton 1980). We verified the electrode positions by using paired-pulse stimulation with a 200-ms inter-stimulus interval (ISI). The LPP and MPP cause paired-pulse facilitation and depression of the fEPSP, respectively (Colino and Malenka 1993).

To investigate the differences in response characteristics between MDs and DDs using rat hippocampal slices, stimuli comprising a train of five constant-voltage pulses

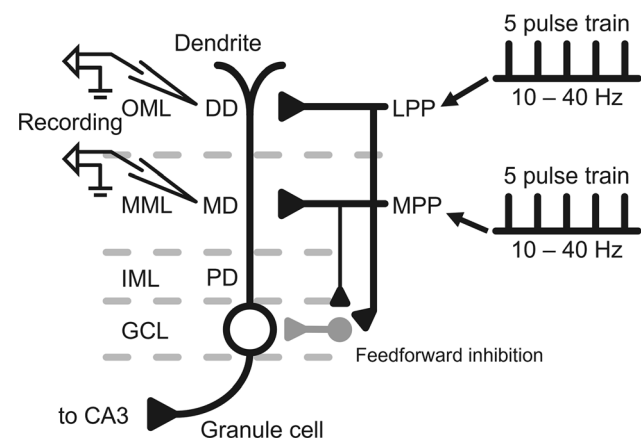


**Fig. 1** Frequency response characteristics of DDs and MDs of GCs. Five electrical stimuli were applied using stimulating electrodes at the LPP or MPP. The stimulus interval was 10–40 Hz. fEPSPs were recorded by a recording electrode. The grey cell indicates feedforward inhibition. *MPP* Medial perforant path, *LPP* Lateral perforant path, *MML* Medial molecular layer, *OML* Outer molecular layer, *IML* Inner molecular layer, *SCL* Granule cell layer, *MDs* Medial dendrites, *DDs* Distal dendrites, *PDs* Proximal dendrites

(pulse duration of 200  $\mu$ s) at 10–40 Hz were applied to the MPP or LPP. The stimulus intensity was less than half of the threshold (Hayakawa et al. 2015). Recording electrodes were made by pulling a microglass tube with a puller (P-97, Sutter Instrument) to obtain a resistance of 3–5 M $\Omega$ . Recording was performed using a patch clamp amplifier (Axopatch 200B, Molecular Devices Corp.), an A/D converter (Digidata 1322A, Molecular Devices Corp.), and recording software (pCLAMP, Molecular Devices Corp.). Recorded fEPSP waveforms acquired through a Gaussian low-pass filter were measured and normalized to the amplitude of the fEPSP of the first stimulation. The NMDA receptor antagonist D-APV (25  $\mu$ M, Sigma) was applied to prevent the frequency stimuli from inducing synaptic plasticity. To investigate the influence of feedforward inhibition from basket cells, picrotoxin (50  $\mu$ M, Sigma), a GABA<sub>A</sub> receptor antagonist, was administered in the ACSF. Statistical analysis was performed using ANOVA.

### GC model with dynamic synapses

To reproduce the response characteristics of GCs obtained from electrophysiological experiments, experiments were performed using a NEURON simulator (Hines and Carnevale 1997). We used the compartmental GC model of the DG with the Hodgkin-Huxley model (Ferrante et al. 2009) as the postsynaptic part, mounting the dynamic synapse model (Tsodyks et al. 1998) to reproduce the inputs to DDs and MDs as the presynaptic part. In the dynamic synapse model, the state transition of neurotransmitters is described by three state variables and four differential equations. The total amount of neurotransmitters in the synaptic transmission is always constant and is expressed by the following equations:

$$\frac{dR(t)}{dt} = \frac{I(t)}{\tau_{rec}} - u(t)R(t)\delta(t - t_{AP}), \quad (1)$$

$$\frac{dE(t)}{dt} = -\frac{E(t)}{\tau_{inact}} + u(t)R(t)\delta(t - t_{AP}), \quad (2)$$

$$\frac{dI(t)}{dt} = -\frac{I(t)}{\tau_{rec}} + \frac{E(t)}{\tau_{inact}}, \quad (3)$$

$$\frac{du(t)}{dt} = -\frac{u(t)}{\tau_{facili}} + Use(1 - u(t))\delta(t - t_{AP}), \quad (4)$$

where the state variables R, E, and I represent the neurotransmitter before release (R), the state released from the presynapse to produce an EPSP (E), and the state until inactivation and reuse (I).  $\delta(t - t_{AP})$  represents the firing of the presynapse and is 1 when the presynaptic cell reaches an action potential.  $u(t)$  is a variable that takes the value 0–1, determined by equation (4). In this case, the neurotransmitter is released from the presynaptic cell, and the time constant  $\tau_{rec}$  is the time constant for recovery when the neurotransmitter is

taken up by the presynaptic cell, state (I).  $\tau_{facili}$  determines the time window for activation by firing at the presynaptic cell. The state variables R, E, and I are determined by the following differential equation, where  $\delta(t - t_{AP})$  is the delta function and represents the presynaptic firing,  $u(t)$  determines the probability of neurotransmitter release at the presynapse, and  $Use$  is a constant that determines the amount of change in the release probability. The membrane potential is determined by the following equations:

$$\frac{dV_m}{dt} = -\left(\frac{1}{C}\right)(I_{in} + I_m), \quad (5)$$

$$I_{in} = g(V_m - E_{rev}), \quad (6)$$

$$I_m = g_{Na}(V_m - E_{Na}) + g_K(V_m - E_K) + g_l(V_m - E_l), \quad (7)$$

where  $I_{in}$  is the current (nA) that is due to the synaptic input,  $I_m$  is the activation equation for Hodgkin-Huxley model. The synaptic weights related to transmission efficiency were set as  $w$ , which was fixed at an appropriate value for effective discrimination for a temporal pattern. The synaptic conductance  $g$  is determined by  $wE(t)$   $\mu$ S.  $g_{Na}$ ,  $g_K$ , and  $g_l$  are the conductances ( $\mu$ S) of the voltage-dependent sodium, potassium, and leak channels, respectively.  $E_{rev}$  is the reversal potential of the EPSP (0 mV).  $E_{Na}$ ,  $E_K$ , and  $E_l$  are the reversal potentials (mV) of the sodium, potassium, and leak channels, respectively.  $C$  is a capacitor in the cell membrane. Before these computational experiments, the peak amplitudes of EPSPs evoked by each pulse were obtained from a soma compartment. The synaptic weights ( $w$ ) of all DDs and MDs were set to 0.0003. We fitted the parameters for the dynamic synapse of DDs and MDs to bring the peak amplitudes of the soma EPSP to a level similar to that of the fEPSPs. The model constructed with these parameters was used without inhibitory input in all computational experiments.

### Computational experiments

First, we investigated the response characteristics of DDs and MDs to random pulse inputs. A total of 100 input sites were randomly created in DDs and MDs in a GC model (Fig. 4a and b). These inputs were generated by Poisson distributions with average frequencies of 1, 5, 10, 20, 25, 30, and 40 Hz and applied for 2 seconds. The synaptic weights ( $w$ ) of DDs and MDs were set to 0.008 and 0.003. The change in the membrane potentials of soma compartments was the response of a GC to each dendritic input.

Next, to investigate the associative information processing of two input MDs and DDs, we performed the following three computational experiments.

- (1) Temporal pattern discrimination for  $\theta$ -burst inputs according to the synaptic weight at MDs

We measured the temporal pattern discrimination of GCs for  $\theta$ -burst inputs with spatial information from the MPP to MDs. The  $\theta$ -burst pulses as inputs to MDs through the MPP were applied to a GC model, which was defined by three parameters: the inter-burst interval (IBI = 125 ms, 8 Hz), the number of pulses in a burst ( $n = 1$ –5), and the pulse interval within a burst (ISI = 5–25 ms) (Fig. 5a). Firing rates for temporal patterns with two parameters ( $n$ , ISI) of a  $\theta$ -burst at 8 Hz were measured in the GC model. Synaptic weights of 0.1, 0.125, and 0.15 were used. The responses of GCs to the  $\theta$ -burst input were evaluated by the average firing rate of the emitted spikes to the execution time (25 seconds).

## (2) Associative effect of excitatory inputs at DDs on the temporal pattern discrimination at MDs

To investigate how the two inputs were associated at MDs and DDs, we applied  $\theta$ -burst pulses and random pulses to the MPP and LPP, respectively (Fig. 6a). The random pulse input varied from 10 to 40 Hz. These inputs were applied for 25 seconds. Additionally, the synaptic weight of DDs was set to 0.11. The response of GCs to  $\theta$ -burst inputs with two parameters ( $n$ , ISI) at 8 Hz was evaluated by the average firing rate of the emitted spikes to the execution time (25 seconds) in the same way as in experiment (1).

## (3) Associative effect of lateral inhibition on the temporal pattern discrimination at MDs

Recently, the existence and role of lateral inhibition in the DG in terms of memory have been reported (Sun et al. 2020; Tuncdemir et al. 2022), and lateral inhibition is 10 times more abundant than recurrent inhibition (Espinoza et al. 2018). Therefore, to investigate the effect of the lateral inhibition of GCs via LPP-derived inputs on the information processing of inputs to MDs, we created a new network model and applied  $\theta$ -burst pulses and random pulses to the MPP and LPP, respectively (Fig. 7a). Inhibitory inputs with three decay times of 5, 10, and 15 ms were respectively applied to the cell body of the GC receiving input from the MPP via an interneuron from the GC receiving input from the LPP. Two inputs for MPP and LPP were applied and the responses of the GCs were evaluated as temporal pattern discrimination in the same way as in experiment (2).

## Results

### Physiological experimental results

#### Frequency response characteristics

To investigate the difference in characteristics of pre-synapse between MPPs and LPPs, five regular pulse stimuli

were applied to MPP and LPP hippocampal GCs to measure the frequency responses of MDs and DDs, respectively. The input frequency was changed from 10 to 40 Hz. Experiments were performed both in the presence and the absence of GABA<sub>A</sub> receptors.

The frequency response results for the five pulse stimuli to DDs are shown in Fig. 2. The magnitudes of the fEPSPs normalized by the peak amplitude of the first input are shown in the presence and absence of inhibitory input (i.e., without and with picrotoxin; *solid circles* and *triangles*) at 10–40 Hz. The paired-pulse facilitation of fEPSPs was observed for the second pulse stimulus both with and without picrotoxin at 10 Hz (Fig. 2a). The magnitudes of the normalized fEPSPs were sustained for the third and subsequent pulse stimuli shown at 10 Hz in the presence of uninhibited GABA<sub>A</sub> receptor (circles). When GABA<sub>A</sub> receptor was blocked by picrotoxin (*triangle*), the paired-pulse facilitation was still observed for the second stimulus, but normalized fEPSPs were transiently decreased for the fourth and fifth pulse stimuli. Moreover, using an input frequency of 20–40 Hz, the paired-pulse facilitation was not observed with GABA<sub>A</sub> receptor (Fig. 2b–e). The magnitudes of normalized fEPSPs for the second and subsequent pulse stimuli were sustained at 20–30 Hz (*solid circles* in Fig. 2b–d) but showed transient responses for the fourth and fifth pulses at 40 Hz (Fig. 2e). When GABA<sub>A</sub> receptor was blocked, the magnitudes of fEPSPs to the third and subsequent stimuli were transiently decreased at 20–40 Hz (*solid triangle* in Fig. 2). These results showed that sustained responses required GABAergic inhibition at DDs.

On the other hand, the frequency response results for the five pulse stimuli to MDs are shown in Fig. 3. Although paired-pulse depression was observed for the second pulse stimulus at 5 Hz, verifying the electrical-stimulating position of the LPP and MPP, they were observed not at 10–25 Hz, but at 30–40 Hz (*solid circle* in Fig. 3). The magnitudes of normalized fEPSPs to the third pulse stimulus were significantly decreased when MDs were stimulated at 10–25 Hz (Fig. 3a–c) and were decreased (transient responses) for the second pulse and subsequent stimuli at 30–40 Hz (Fig. 3d and e), both with and without significance. Thus, the frequency responses for the five pulse stimuli to MDs were transiently decreased, which was not related to GABAergic inhibition.

After the physiological experiments, to investigate the associative information processing between inputs to MDs and DDs in the DG, we performed computational experiments in a GC model using NEURON simulator with a dynamic synapse model, fitted to our physiological experimental data. The results of the model fitting are shown in Table 1. It was confirmed that the time constant  $\tau_{\text{rec}}$  (2965 ms) for the recovery of the MPP site was larger



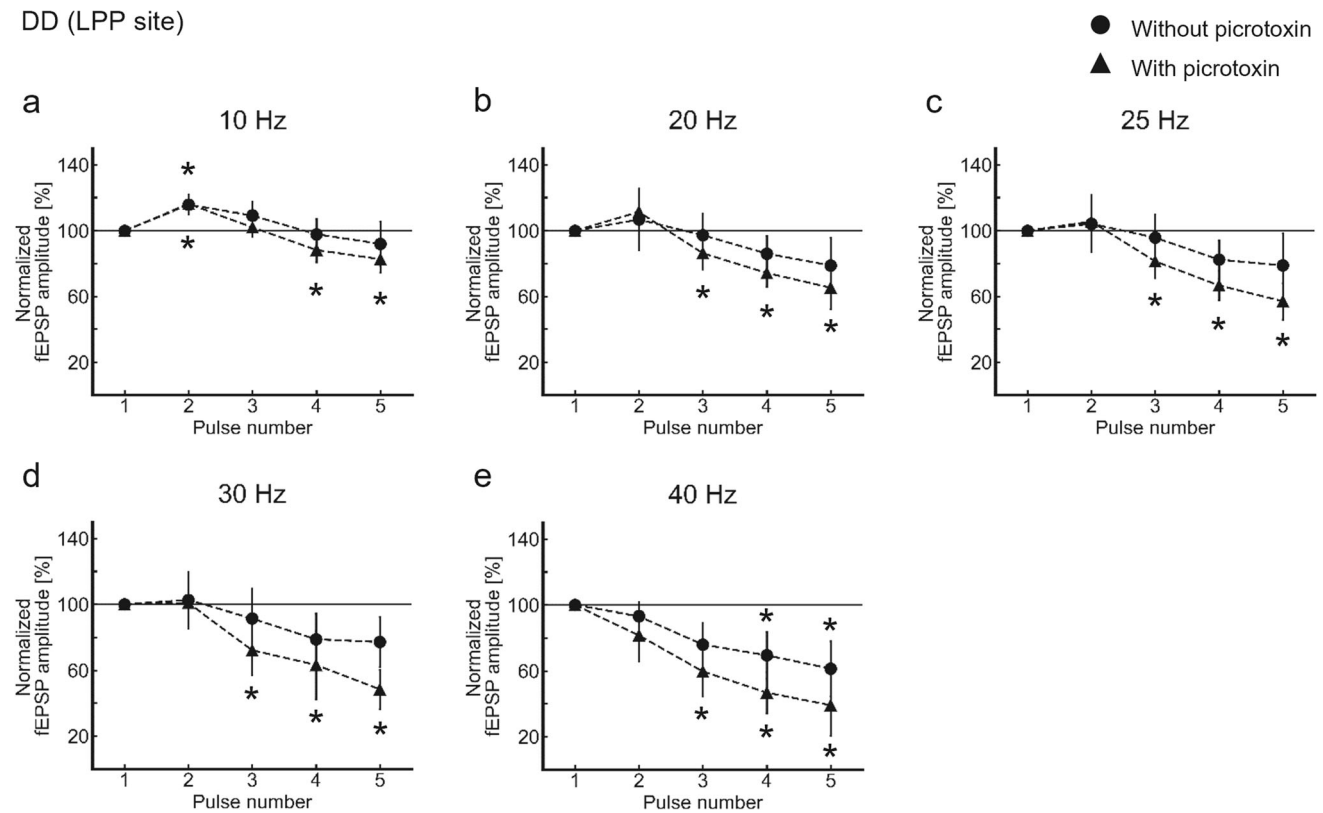


**Fig. 2** Frequency response characteristics of DDs. **a–e** The response is the mean  $\pm$  S.E.M. of the peak value of the amplitude of the fEPSP normalized by the first response. Black circles indicate the control while black triangles indicate the picrotoxin-treated condition. The LPP was stimulated at **a** 10 Hz (Control+D-APV,  $n = 8$ ,  $p = 0.002$ ; Control+D-APV+picrotoxin,  $n = 8$ ,  $p < 0.001$ ), **b** 20 Hz (Control+D-APV,  $n = 8$ ,  $p = 0.009$ ; Control+D-APV+picrotoxin,  $n = 8$ ,  $p < 0.001$ ), **c** 25 Hz (Control+D-APV,  $n = 8$ ,  $pp = 0.022$ ; Control+D-

APV+picrotoxin,  $n = 8$ ,  $p < 0.001$ ), **d** 30 Hz (Control+D-APV,  $n = 8$ ,  $p = 0.017$ ; Control+D-APV+picrotoxin,  $n = 8$ ,  $p < 0.001$ ), and **e** 40 Hz (Control+D-APV,  $n = 8$ ,  $p = 0.001$ ; Control+D-APV+picrotoxin,  $n = 8$ ,  $p < 0.001$ ). The upper and lower symbols “\*” indicate a significant difference between the fEPSP for the first stimulus and the fEPSPs for the second and subsequent stimuli for without and with picrotoxin, respectively.  $*p < 0.05$

than that of the LPP site (243 ms). This indicates, in physiological experiments, that normalized EPSPs transiently decrease for successive inputs to MDs due to the slow recovery of MPP neurotransmitters and that DDs show sustained responses due to the rapid recovery of neurotransmitters.

## Computational experiment results

### Response characteristics of DDs and MDs

First, we investigated the response characteristics of DDs and MDs to random pulse inputs. A total of 100 input sites were randomly created in DDs and MDs (Fig. 4a and b). These inputs were generated by Poisson distributions with average frequencies of 1, 5, 10, 20, 25, 30, and 40 Hz for 2 seconds. The membrane potential was measured from the GC cell body. DDs showed a sustained response according to the input frequency (Fig. 4c), with high-frequency inputs resulting in a high membrane potential that was maintained

for the duration of the input. In contrast, in MDs, high-frequency inputs transiently induced a high membrane potential at the onset of the input, but the membrane potential decreased rapidly on the same time scale, regardless of the input frequency (Fig. 4d). Therefore, high-frequency random pulse inputs to DDs persistently maximize the response of GCs, which show a property suitable for “rate coding”. In contrast, the response of GCs is maximized by intermittent high-frequency burst inputs to MDs, which show a property suitable for “temporal coding”.

### Associative information processing of two input MDs and DDs

Next, to investigate the associative information processing of two input MDs and DDs, we performed three computational experiments: (1) the temporal pattern discrimination for  $\theta$ -burst inputs depending on the synaptic weight at MDs, (2) the effect of DD inputs on the temporal pattern

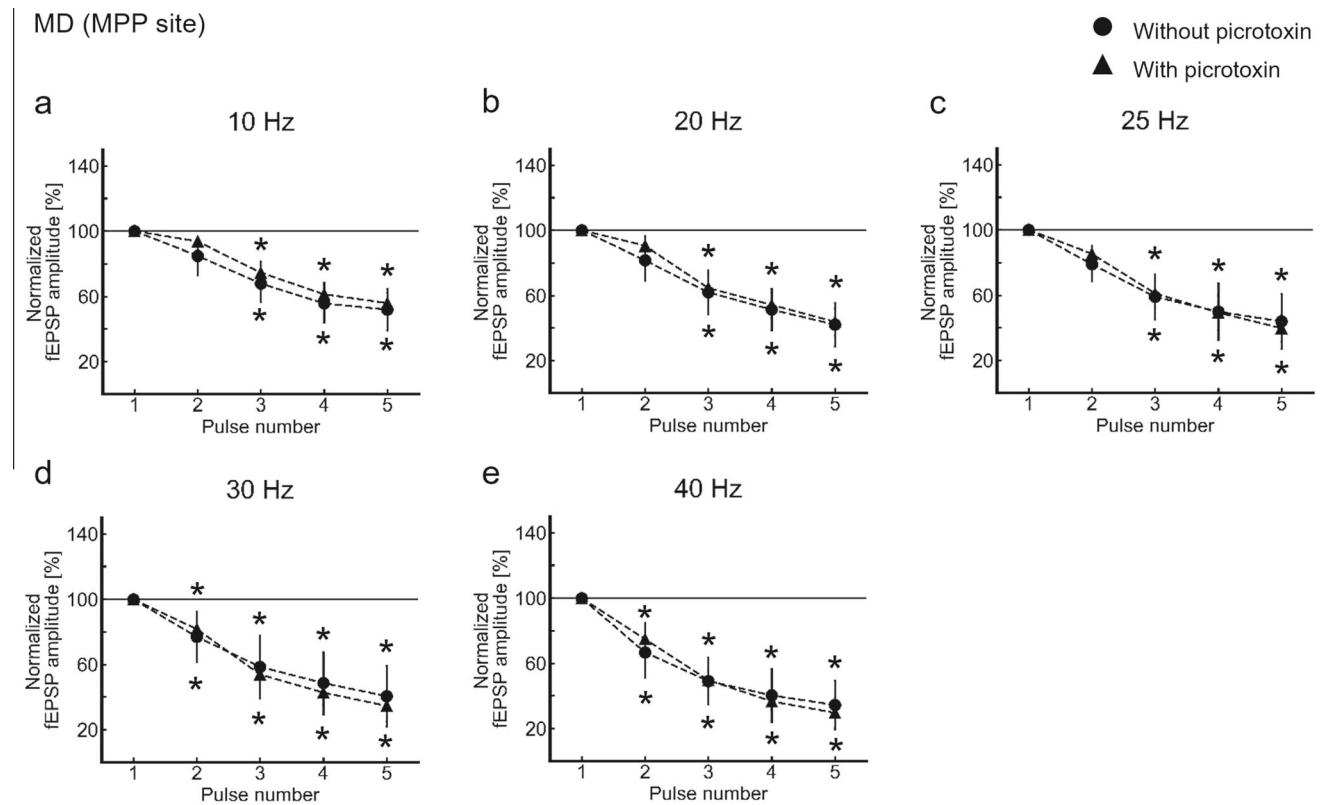


**Fig. 3** Frequency response characteristics of MDs. **a–e** The response is the mean  $\pm$  S.E.M. of the peak value of the amplitude of the fEPSP normalized by the first response. Black circles indicate the control while black triangles indicate the picrotoxin-treated condition. The MPP was stimulated at **a** 10 Hz (Control+D-APV,  $n = 8$ ,  $p < 0.001$ ; Control+D-APV+picrotoxin,  $n = 8$ ,  $p < 0.001$ ), **b** 20 Hz (Control+D-APV,  $n = 8$ ,  $p < 0.001$ ; Control+D-APV+picrotoxin,  $n = 8$ ,  $p < 0.001$ ), **c** 25 Hz (Control+D-APV,  $n = 8$ ,  $p < 0.001$ ;

Control+D-APV+picrotoxin,  $n = 8$ ,  $p < 0.001$ ), **d** 30 Hz (Control+D-APV,  $n = 8$ ,  $p < 0.001$ ; Control+D-APV+picrotoxin,  $n = 8$ ,  $p < 0.001$ ), and **e** 40 Hz (Control+D-APV,  $n = 7$ ,  $p < 0.001$ ; Control+D-APV+picrotoxin,  $n = 8$ ,  $p < 0.001$ ). The upper and lower symbols “\*” indicate a significant difference between the fEPSP for the first stimulus and the fEPSPs for the second and subsequent stimuli for without and with picrotoxin, respectively.  $*p < 0.05$

**Table 1** Parameters for LPP and MPP sites

	LPP site	MPP site
$\tau_{rec}$ (ms)	243	2965
$\tau_{in}$ (ms)	1	1
$\tau_{facili}$ (ms)	499	1
$U$	0.5	0.3

$\tau_{rec}$  is the time constant for recovery when the neurotransmitter is taken up by the presynaptic cell.  $\tau_{in}$  is the time constant of the state until inactivation and reuse (I).  $\tau_{facili}$  determines the time window for activation by firing at the presynaptic cell.

discrimination for  $\theta$ -burst inputs at MDs, and (3) the effect of lateral inhibition on the temporal pattern discrimination for  $\theta$ -burst inputs at MDs. MDs and DDs showed different characteristics, namely, temporal and rate coding, respectively (Fig. 4c and d). In addition, MDs receive spatial (place) information in  $\theta$  rhythm from the EC (O’Keefe and Recce 1993; Skaggs et al. 1996; Igarashi et al. 2014).

Therefore, we first examined the response to the temporal pattern of  $\theta$ -burst inputs to MD synapses, suitable for temporal coding, and then examined the effect of input to DD synapses, suitable for rate coding, on the temporal pattern discrimination at MDs.

#### (1) Temporal pattern discrimination for $\theta$ -burst inputs according to synaptic weight at MDs

First, to determine the most effective temporal pattern (burst) for GC activation at MDs where spatial (place) information was translated on  $\theta$  rhythm, we applied  $\theta$ -burst inputs to MDs, with variations in the IBI, ISI, and number of pulses (Fig. 5a). Three synaptic weights—0.1 (weak), 0.125 (medium), and 0.15 (strong)—were used.

When the synaptic weight at MDs was 0.1, broad input patterns were observed at a low firing rate (Fig. 5b). When the MD weight was 0.125, effective temporal patterns ( $n = 5$ , ISI = 7 and 8) were discriminated at a moderate firing rate (Fig. 5c). Furthermore, when the MD weight was 0.15, responses were facilitated for additional temporal

**Fig. 4** Responses of DDs and MDs to random inputs. **a, b** The blue dots indicate **a** DD and **b** MD synaptic connections, respectively. For presynapses, the dynamic synaptic model of Tsodkys et al. was used. For postsynapses, the compartmental granule cell model of Ferrante et al. was used with the Hodgkin-Huxley model. **c** DDs and **d** MDs were subjected to random pulse inputs of 10–40 Hz for 2 seconds. Membrane potentials were measured from the cell body of the compartment model of GCs

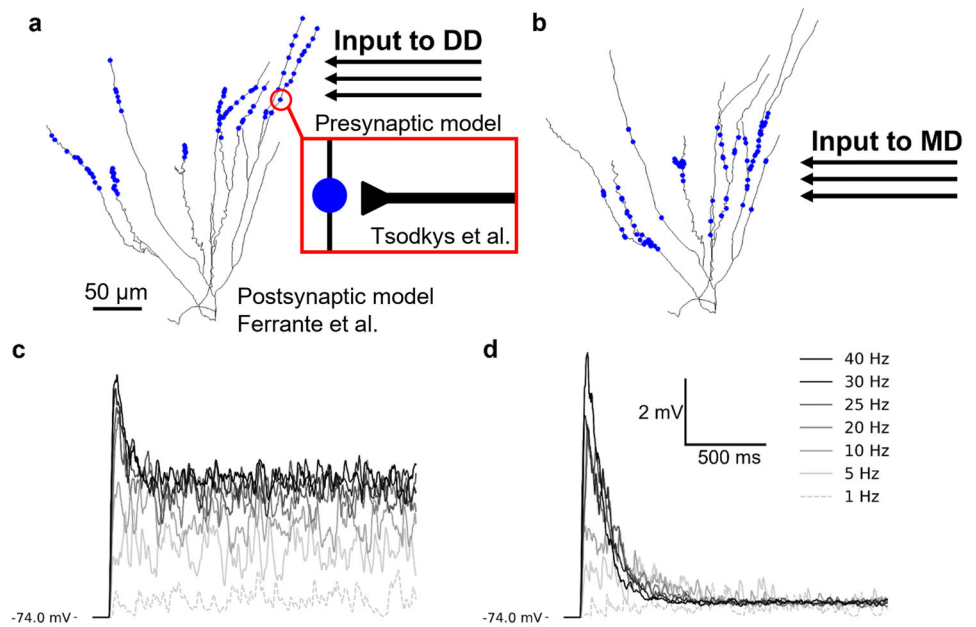
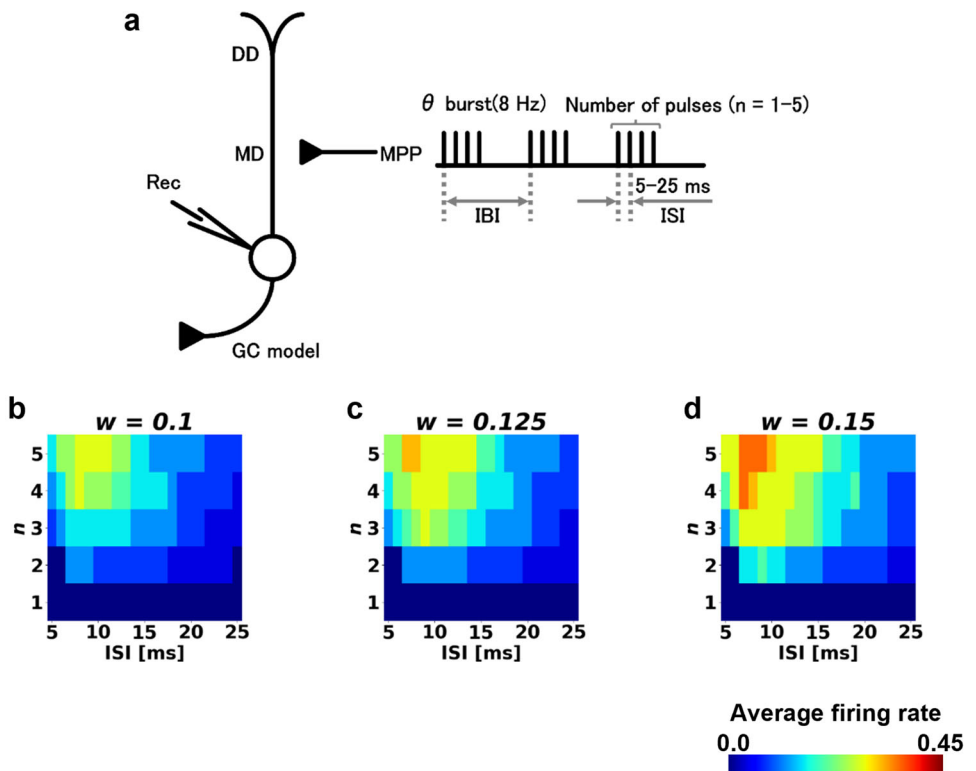


**Fig. 5** Responses of GCs to  $\theta$ -burst inputs applied to MDs. **a** Regular burst pulse inputs were applied to MDs. The ISI (inter-stimulus interval) and the number of pulses were changed from 5 to 25 ms and from 1 to 5, respectively. The IBI (inter-burst interval) was 125 ms (8 Hz). These inputs were applied for 25 seconds. **b–d** The MPP-MD weight was changed from **(b)** 0.1, to **(c)** 0.125, and to **(d)** 0.15. The response of the GC to the  $\theta$ -burst input was evaluated by the average firing rate of the emitted spikes during the execution time (25 seconds)

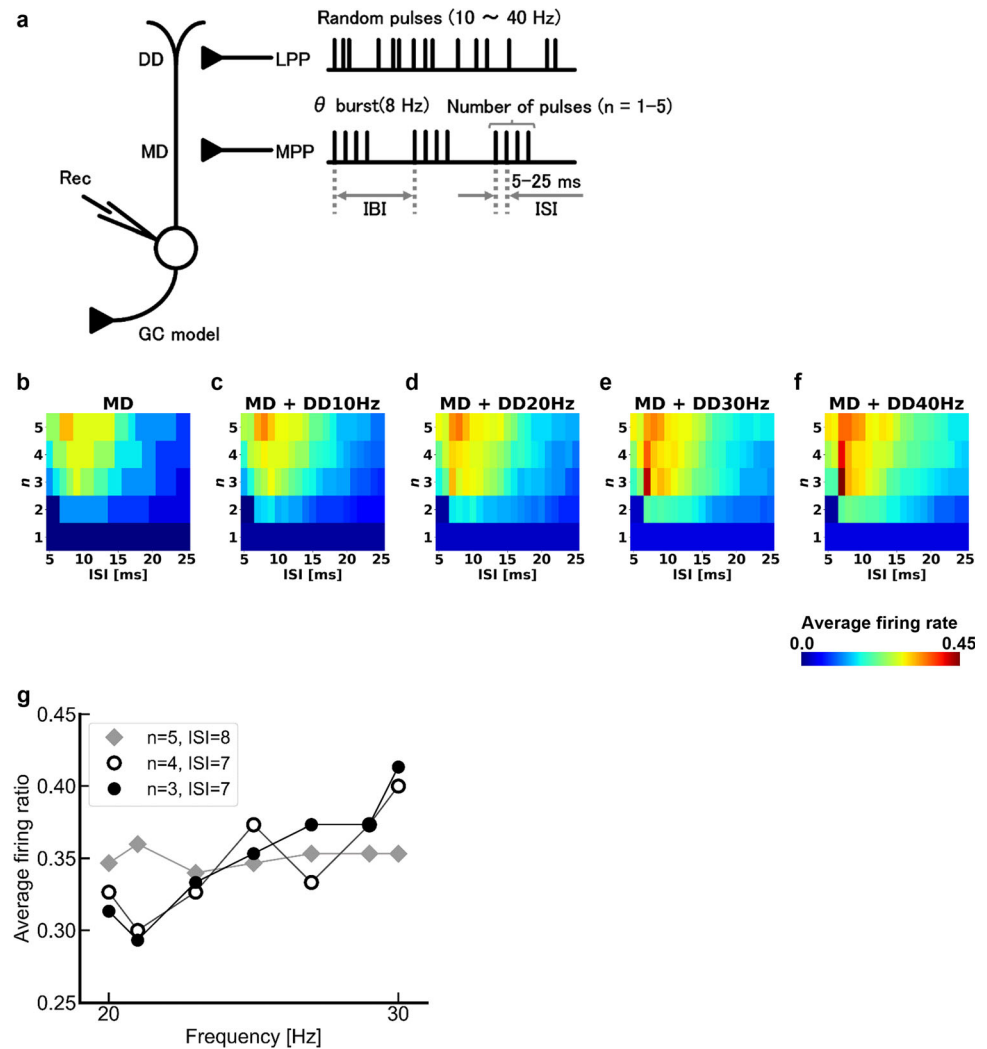


patterns and the sensitivity to the input patterns was broadened and less specific ( $n = 4$ ,  $ISI = 7$  to  $8$  and  $n = 5$ ,  $ISI = 7$  to  $9$ ) (Fig. 5d). Based on these results,  $w = 0.125$  showed effective discrimination for a temporal pattern (burst) for GC activation and we thus used it as the MD fixed weight in the subsequent experiments.

- (2) Associative effect of excitatory inputs at DDs on the temporal pattern discrimination for  $\theta$ -burst inputs at MDs

Second, to investigate how the two inputs were associated at MDs and DDs, we applied  $\theta$ -burst pulses (8 Hz) with two parameters,  $n$  and ISI, and Poison random pulses

**Fig. 6** Responses of GCs to  $\theta$ -burst input from the MPP enhanced by random pulses from the LPP. **a** Regular burst pulse inputs and random pulse inputs were applied to MDs and DDs, respectively. The ISI (inter-stimulus interval) and the number of pulses were changed from 5 to 25 ms and from 1 to 5, respectively. The IBI (inter-burst interval) was 125 ms (8 Hz). The response of the GC to the  $\theta$ -burst input was evaluated by the average firing rate of the emitted spikes to the execution time (25 seconds). **b–f** Responses of a GC model to the application of **b**  $\theta$ -burst inputs only, **c**  $\theta$ -burst inputs+10-Hz random pulse, **d**  $\theta$ -burst inputs+20-Hz random pulse, **e**  $\theta$ -burst inputs+30-Hz random pulse, and **f**  $\theta$ -burst inputs+10-Hz random pulse. **g** The time pattern of the  $\theta$ -burst depended on the frequency of the DD input, as shown by the transition of the three effective patterns



(10–40 Hz) to the MPP and LPP (Fig. 6a) and measured the effect of random inputs to DDs on the firing rate of GCs for different temporal patterns of  $\theta$ -burst inputs to MDs (Fig. 6c–f). During the experiments, the synaptic weights of the MDs and DDs were fixed at 0.125 and 0.11, respectively.

When the MDs of GCs were administered  $\theta$ -burst inputs, effective temporal patterns ( $n = 5, \text{ISI} = 7$  and  $8$ ) for GC activation were observed (Fig. 5c and 6b). When 10-Hz random pulse inputs to the DDs were additionally given for  $\theta$ -burst inputs to MDs in GCs, the GCs were effectively activated by the specific input pattern ( $n = 5, \text{ISI} = 8$ ) (Fig. 6c). Moreover, with the application of additional random pulse inputs at 20 Hz to DDs, new effective temporal patterns of  $\theta$ -burst inputs ( $n = 4, 3, \text{ISI} = 7$ ) of MDs to activate the GC were observed (Fig. 6d). Next, the application of additional random pulse inputs at 30 or 40 Hz to DDs (Fig. 6e and f) shifted the most effective temporal pattern of MD input to a  $\theta$ -burst input ( $n = 3, \text{ISI} = 7$ ), while maintaining effective

temporal patterns ( $n = 5, \text{ISI} = 8$  and  $n = 4, \text{ISI} = 7$ ). These results showed that one specific pattern of  $\theta$ -burst inputs ( $n = 5, \text{ISI} = 8$ ) was enhanced by DD inputs at 10–20 Hz while, at over 30 Hz, the effective temporal patterns became broad ( $n = 5, \text{ISI} = 8$  and  $n = 3-4, \text{ISI} = 7$ ), although the most effective  $\theta$ -burst pattern was  $n = 3$  and  $\text{ISI} = 7$ . To illustrate the detailed transition of the time pattern of  $\theta$ -burst inputs depending on the frequency of the DD input, the transition of the three effective patterns ( $n = 5, \text{ISI} = 8$  and  $n = 3-4, \text{ISI} = 7$ ) is shown in detail in Fig. 6g for frequencies from 20 Hz to 30 Hz. The temporal pattern of a  $\theta$ -burst input of  $n = 5$  and  $\text{ISI} = 8$  was most effective at 20 Hz. A transition from a  $\theta$ -burst of  $n = 5$  and  $\text{ISI} = 8$  to a  $\theta$ -burst of  $n = 3-4$  and  $\text{ISI} = 7$  was observed over 20 Hz to 40 Hz. These three patterns were retained, each with greater effect. Thus, the results showed that the temporal pattern sensitivities of GCs for burst inputs to MDs was modulated by boosting of the GC activation, caused of rate coding depending on the frequency of the random pulse inputs applied to the DDs.



(3) Associative effect of lateral inhibition on the temporal pattern discrimination at MDs

Finally, because the crucial roles of lateral inhibition in GCs were recently reported (Tuncdemir et al. 2022), we investigated the effect of lateral inhibition derived via interneurons from the LPP on the information processing of MD inputs. We created a new network model of GCs with lateral inhibition, as shown in Fig. 7a. As in experiments (1) and (2),  $\theta$ -burst inputs were applied to the MDs of the GC from the MPP. On the other hand, random inputs were applied to the DDs of the other GCs from the LPP at 10–40 Hz, which was transported to the recording GCs as lateral inhibitory input via interneurons. Three decay times of lateral inhibition (5, 10 and 15 ms) were used.

When the MDs of the GCs were administered  $\theta$ -burst inputs, effective temporal patterns ( $n = 5$ , ISI = 7–8) for GC activation were observed (Figs. 5c and 7b). Firstly, when lateral inhibition with a decay time of 5 ms induced by 10-Hz random pulse inputs to the DDs were additionally given for  $\theta$ -burst inputs to MDs in GCs, the GCs were effectively activated by the specific input pattern ( $n = 5$ , ISI = 8) (Fig. 7c, panel 1) in broader pattern ( $n = 5$ , ISI = 7–9). Next, with the application of additional random pulse inputs at 20 Hz to DDs, the effective temporal pattern was returned to the origin ( $n = 5$ , ISI = 7–8) (Figs. 7b and 7c, panel 2). Moreover, with the application of additional random pulse inputs at 30 Hz and 40 Hz, the effective temporal pattern was broader at 30 Hz ( $n = 5$ , ISI = 7–9) (Fig. 7c, panel 3) then returned to the origin at 40 Hz ( $n = 5$ , ISI = 7–8) (Fig. 7c, panel 4). These results showed that one specific pattern of  $\theta$ -burst inputs ( $n = 5$ , ISI = 8) was enhanced by DD inputs at 10 Hz, while maintaining effective temporal patterns ( $n = 5$ , ISI = 7–8) at another frequency. Secondly, when lateral inhibition with the decay of 10 ms induced by 10-Hz random pulse inputs to the DDs were additionally given for  $\theta$ -burst inputs to MDs in GCs, the GC response was still activated by the same specific input pattern ( $n = 5$ , ISI = 7–8) (Fig. 7d, panel 1) as the origin (Fig. 7b). Moreover, with the application of additional random pulse inputs at 20 Hz to DDs, the effective temporal patterns of  $\theta$ -burst of MD input to activate GCs was tuned up to a single temporal pattern ( $n = 5$ , ISI = 7) (Fig. 7d, panel 2). Next, with the application of additional random pulse inputs at 30 Hz and 40 Hz to DDs (Fig. 7d, panels 3–4), the most effective temporal pattern of MD input was shifted to a  $\theta$ -burst of  $n = 5$  and ISI = 8 and the firing rate peaked at 30 Hz, while maintaining effective temporal patterns ( $n = 5$ , ISI = 7). Accordingly, the results showed that the IBI of  $\theta$ -burst inputs to MDs became longer as the DD input frequency increased to 30 Hz, where GC activity was maximal, and then returned to the origin at 40 Hz. Lastly, when lateral inhibition with a decay

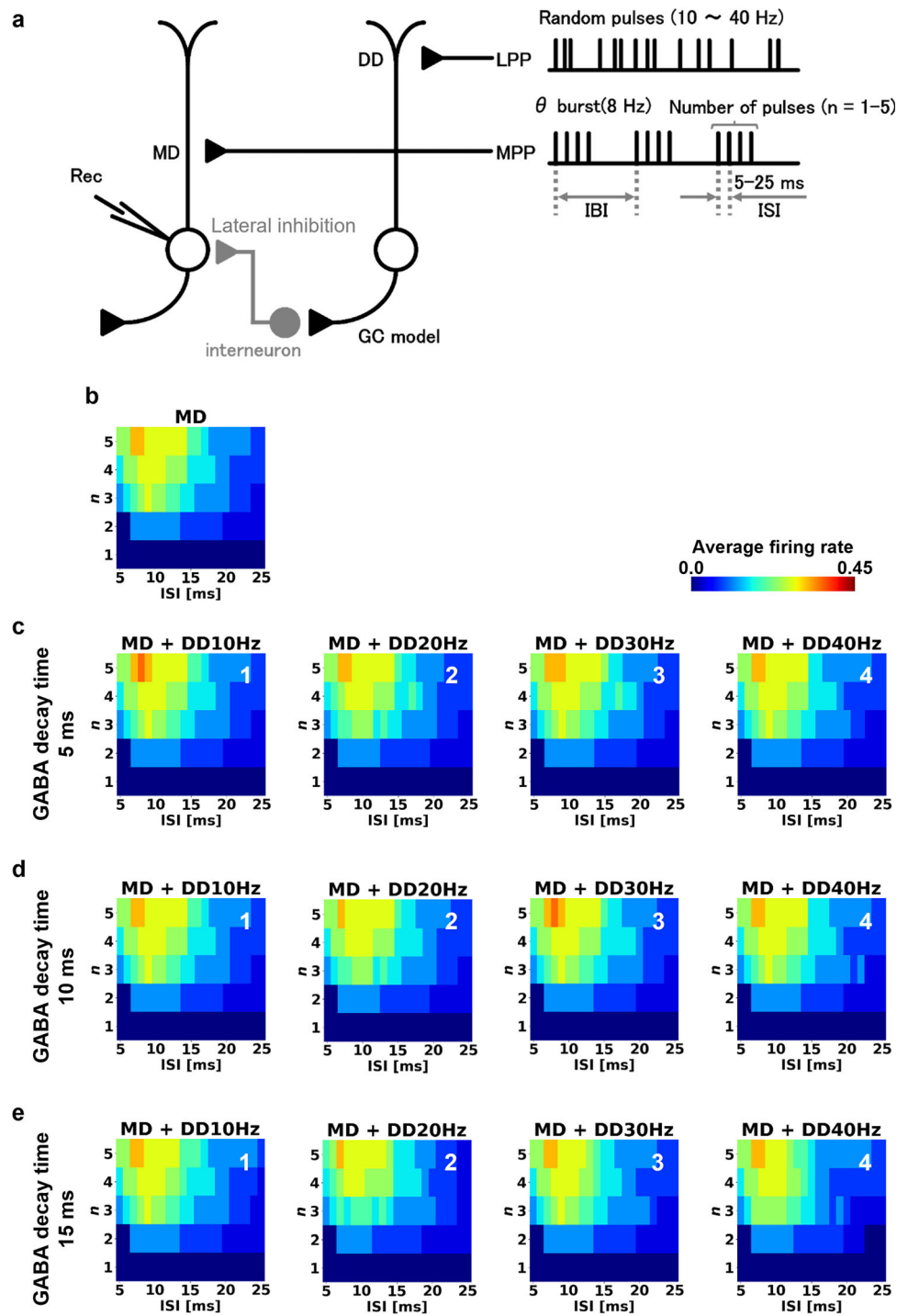
time of 15 ms induced by 10-Hz random pulse inputs to the DDs was additionally given for  $\theta$ -burst inputs to MDs in GCs, the GC response was activated by the same specific input pattern ( $n = 5$ , ISI = 7–8) (Fig. 7e, panel 1) as the origin (Fig. 7b). Moreover, with the application of additional random pulse inputs at 20 Hz to DDs, the effective temporal patterns of  $\theta$ -burst of MD input to activate GCs was tuned up to a single temporal pattern ( $n = 5$ , ISI = 7) (Fig. 7e, panel 2). Next, with the application of additional random pulse inputs at 30 Hz and 40 Hz to DD, the effective temporal patterns were returned to the origin ( $n = 5$ , ISI = 7–8) (Figs. 7b and 7e, panel 3–4). These results showed that one specific pattern of  $\theta$ -burst inputs ( $n = 5$ , ISI = 8) was observed by DD inputs at 20 Hz, while maintaining the same effective temporal patterns ( $n = 5$ , ISI = 7–8) at 10, 30 and 40 Hz as the origin.

## Discussion

To investigate associative information processing between inputs to MDs and DDs in GCs, we first measured the frequency responses of MDs and DDs in rat hippocampal slices using electrophysiological experiments. Next, we performed computer simulation using a dynamic synapse model on a multi-compartment model of GCs, fixed by parameter fitting with our physiological data. The application of  $\theta$ -burst inputs to MDs and random pulses to DDs in a network with or without lateral inhibition revealed the effect of random inputs to DDs on the temporal pattern discrimination of  $\theta$ -burst inputs at MDs.

In the physiological experiments, successive electrical stimuli were applied to the LPP or MPP from 10 to 40 Hz to examine the frequency response characteristics of DDs and MDs. Different responses to paired-pulse stimuli were observed in the two synapses at 5 Hz, which indicated two stimulation sites for LPP-DD synapses with paired-pulse facilitation and MPP-MD synapses with paired-pulse depression, in line with the results of a previous report (Colino and Malenka 1993). The paired-pulse facilitation was also observed for the second input to the LPP-DD synapse at 10 Hz (Fig. 2a). In addition, DDs showed a sustained response at 10–30 Hz (Fig. 2a–d) but not at 40 Hz (Fig. 2e). Furthermore, when the inhibitory input was blocked, DDs did not show sustained responses at any input frequencies (Fig. 2a–e). These results suggest that DDs have sustained responses to inhibitory input, depending on the input frequency. On the other hand, MDs showed transient responses regardless of input frequency and the presence or absence of inhibitory cells (Fig. 3a–e). It was previously reported that the feedforward inhibition induced by the MPP to MDs was smaller than that induced by the LPP to DDs (Ceranik et al. 1997; Booker and Vida

**Fig. 7** Responses of GCs to pulsed input to GCs receiving input from the MPP when inhibited by lateral inhibition of GCs receiving input from the LPP. **a** Recently, the existence and role of lateral inhibition in the DG in terms of memory have recently been studied (Sun et al. 2020; Tuncdemir et al. 2022). A network was created in which the GC receiving input from the LPP blocks the response of the GC receiving input from the MPP by lateral inhibition. For presynapses, the dynamic synaptic model by Tsodyks et al. was used. For postsynapses, the compartmental granule cell model by Ferrante et al. was used with the Hodgkin-Huxley model. Regular burst pulse inputs and random pulse inputs were applied to MDs and DDs, respectively. The ISI (inter-stimulus interval) and the number of pulses were changed from 5 to 25 ms and 1 to 5, respectively. The IBI (inter-burst interval) was 125 ms (8 Hz). The response of the GC to the  $\theta$ -burst input was evaluated by the average firing rate of the emitted spikes to the execution time (25 seconds). **b** Responses of a GC model to the application of  $\theta$ -burst inputs only. **c–e** GABA decay time was changed at **c** 5 ms, **d** 10 ms and **e** 15 ms. Responses of a GC model to the application of (panel 1)  $\theta$ -burst inputs+10-Hz random pulse, (panel 2)  $\theta$ -burst inputs+20-Hz random pulse, (panel 3)  $\theta$ -burst inputs+30-Hz random pulse, and (panel 4)  $\theta$ -burst inputs+10-Hz random pulse



2018). Accordingly, these results suggest that feedforward inhibition modulates the synaptic properties of DDs and promotes a sustained response, in addition to the distinct presynaptic properties of LPP-DDs and MPP-MDs.

After the physiological experiments, to conduct computational experiments in a dynamic synapse model of GCs using NEURON simulator, the dynamic synapse model was fitted to the data obtained from our physiological

experiments. The  $\tau_{\text{facil}}$  value, as the firing activation window, was larger for LPP-DD synapses (499 ms) than for MPP-MD synapses (1 ms) (Table 1), which caused paired-pulse facilitation only at DDs. The  $\tau_{\text{rec}}$  value was large for MPP-MD synapses (2945 ms) because there was insufficient time to collect the neurotransmitter, which was thought to result in transient response characteristics to a successive pulse train. The  $\tau_{\text{rec}}$  value was small for LPP-

DD synapses (243 ms) (Table 1), indicating that the neurotransmitter recovered quickly, resulting in sustained response characteristics to a continuous pulse train.

At the beginning of the computational experiments, the response characteristics of DDs and MDs to random pulse inputs were measured by fitting our experimental data to a dynamic synapse model of GCs. When the LPP was administered a random pulse input of 2-second duration at 1–40 Hz, the GC showed a sustained response. Furthermore, the membrane potential of the GC increased with an increasing input frequency (Fig. 4c). This result suggests that the input from the LPP exerts “rate coding” to increase the membrane potential of GCs. On the other hand, when the MPP was subjected to a random pulse input of 2-second duration at 1–40 Hz, the GC membrane potential showed a transient increase, but the GC membrane potential decreased depending on the number of input pulses (Fig. 4e). This result suggests that the MPP-MD synapse has suitable characteristics for detecting temporal timing, such as that of input sequences comprising burst “temporal coding” (Buzsáki 2002).

Next, to investigate the associative information processing of two input MDs and DDs, we first examined the temporal pattern discrimination for  $\theta$ -burst input depending on the synaptic weight at MDs, then the effects of DD inputs on the temporal pattern discrimination for  $\theta$ -burst input at MDs, and finally the effects of lateral inhibition on the temporal pattern discrimination for  $\theta$ -burst input at MDs.

First, to determine the most effective temporal pattern (burst) for GC activation at MDs where spatial (place) information was translated on  $\theta$  rhythm, we applied  $\theta$ -burst input to MDs, with the response determined by the IBI, ISI, and number of pulses (Fig. 5a). As the synaptic weight at MDs increased, broad input patterns with a low firing rate were observed (Fig. 5b), with effective  $\theta$ -burst ( $n = 5$ ,  $ISI = 7$  and  $8$ ) observed at the medium firing rate (Fig. 5c) and finally broadened temporal patterns with a high firing rate (Fig. 5d). These results suggest that the GC activated in response to specific firing patterns of the  $\theta$ -burst input from the MPP. Therefore, in the subsequent experiments, we used a medium synaptic weight (0.125) for estimating temporal pattern discrimination.

Next, we examined the influence of the frequency of the random pulse input to DDs on the temporal pattern discrimination of  $\theta$ -burst input to MDs in GCs. The temporal pattern of  $\theta$ -burst ( $n = 5$ ,  $ISI = 8$ ) was most effective at 21 Hz, with a transition from a  $\theta$ -burst of  $n = 5$  and  $ISI = 8$  to a  $\theta$ -burst of  $n = 3$ – $4$  and  $ISI = 7$  observed from 20 to 40 Hz (Fig. 6c–g). Thus, the temporal pattern sensitivity of GCs for burst inputs to MDs depended on the frequency of the random pulse inputs applied to DDs, with these three patterns being retained with the greatest ability to activate

GCs. The results suggest that GCs have MD synapses tuned for a temporal pattern of  $\theta$ -burst input and are able to fire with fewer pulses in a burst as the frequency of DD inputs increases. In addition, GCs receive inputs through LPP and MPP synapses (Alonso and García-Austt 1987; Igarashi et al. 2007; Deshmukh et al. 2010), which is consistent with the inputs to each dendrite that activate a GC. In addition, LEC neurons show irregular activity compared with MEC neurons (Deshmukh et al. 2010), which in turn show regular burst input at  $\theta$  intervals (Alonso and Garcia-Austt 1987; Deshmukh et al. 2010). Accordingly, our results suggest that GCs regulate the input pattern discrimination of  $\theta$ -burst inputs from MDs according to the input from DDs. Indeed, GCs selectively react to inputs at  $\theta$  frequency (Ishizuka et al. 2004). Previous  $\theta$ -phase gamma-amplitude coupling analysis revealed that gamma-frequency activity (100–150 Hz) in MECs was phase-locked to the trough phase of the  $\theta$  cycle (Fernández-Ruiz et al. 2021). The frequency of the pulse within the  $\theta$ -burst input used in this study is approximately 142.9 Hz when the ISI is 7 ms and 125 Hz when the ISI is 8 ms. This is consistent with the MEC pattern found in the report by Fernández-Ruiz et al. Interestingly, the ability of a frequency of 21 Hz to induce the most effective pattern— $\theta$ -burst of  $n = 5$  and  $ISI = 8$ —is consistent with the frequency previously observed during the cue sampling period (Igarashi et al. 2014). This may indicate that the MPP-MD synapse has suitable inherent characteristics for information processing for certain  $\theta$ -bursts. In addition, we consider that the pulse number of bursts comprising a  $\theta$ -burst was reduced from five to three by frequency-dependent boosting induced by direct random input to LPP-DD synapses, allowing for efficient GC activation.

Finally, we created a network in which lateral inhibition would work via interneurons from the GC receiving input from the LPP to the GC receiving input from the MPP. We examined the effect of lateral inhibition derived via interneurons from the LPP on the information processing of MD inputs because the crucial roles of lateral inhibition in GCs were recently reported (Tuncdemir et al. 2022). In the experiment, using three decay times (5, 10, and 15 ms) in the lateral inhibition, an effective theta burst patterns to MD were measured. Firstly, with the decay time of 5 ms, one specific pattern of  $\theta$ -burst inputs ( $n = 5$ ,  $ISI = 8$ ) was enhanced by DD inputs at 10 Hz, while maintaining effective temporal patterns ( $n = 5$ ,  $ISI = 7$ – $8$ ) at another frequency. Next, with the decay time of 10 ms, the effective  $\theta$ -burst pattern was observed at 30 Hz (Fig. 7d, panels 1 to 4). On the other hand, with the decay time of 15 ms, one specific pattern of  $\theta$ -burst inputs ( $n = 5$ ,  $ISI = 7$ ) was appeared by DD inputs at 20 Hz, although the firing rate was not increased, while maintaining the same effective temporal patterns ( $n = 5$ ,  $ISI = 7$ – $8$ ) at 10, 30 and 40 Hz as

the origin. Consequently the effective theta burst pattern changed depending on the decay time of the lateral inhibition caused by LPP input frequency. The result suggests that the sensitivity of temporal pattern discrimination was enhanced by the lateral inhibition via interneurons from around GCs receiving input from the LPP, depending on the input frequency from LPP. It is likely that the pattern discrimination of GCs for the  $\theta$ -burst pattern from the MPP was associatively regulated depending on the local network with lateral inhibition. Meanwhile, interestingly, when lateral inhibition with the decay time of 10 ms (Ferrante et al. 2009) or 15ms was applied, one specific pattern of  $\theta$ -burst inputs ( $n = 5$ ,  $ISI = 7$ ) tuned up with an LPP input of 20 Hz (Figs. 7d, panel 2 and 7e, panel 2).

Accordingly, our findings demonstrated that the suitable temporal pattern of GC activation for burst inputs to MDs was enhanced or tuned up by the lateral inhibition by around GCs activation caused of input from LPP, and boosted by DD input from LPP. It has been reported that smell promotes recall of reward locations in behavioral experiments in rats. Our results suggest that the temporal pattern sensitivity of spatial information processing of GCs for temporal pattern inputs through MPP from EC is associatively modified by the non-spatial input information, like smell, though LPP from EC.

**Funding** The Japan Society for the Promotion of Science (JSPS) KAKENHI Grant Numbers (JP16K00405 and JP19K12223)

## References

- Alonso A, García-Aust E (1987) Neuronal sources of theta rhythm in the entorhinal cortex of the rat. II. Phase relations between unit discharges and theta field potentials. *Exp Brain Res* 67:502–509. <https://doi.org/10.1007/BF00247283>
- Booker SA, Vida I (2018) Morphological diversity and connectivity of hippocampal interneurons. *Cell Tissue Res* 373:619–641. <https://doi.org/10.1007/s00441-018-2882-2>
- Burwell RD, Amaral DG (1998) Perirhinal and postrhinal cortices of the rat: interconnectivity and connections with the entorhinal cortex. *J Comp Neurol* 391:293–321. [https://doi.org/10.1002/\(sici\)1096-9861\(19980216\)391:3%3c293::aid-cne2%3e3.0.co;2-x](https://doi.org/10.1002/(sici)1096-9861(19980216)391:3%3c293::aid-cne2%3e3.0.co;2-x)
- Buzsáki G (2002) Theta oscillations in the hippocampus. *Neuron* 33:325–340. [https://doi.org/10.1016/s0896-6273\(02\)00586-x](https://doi.org/10.1016/s0896-6273(02)00586-x)
- Ceranik K, Bender R, Geiger JR et al (1997) A novel type of GABAergic interneuron connecting the input and the output regions of the hippocampus. *J Neurosci Off J Soc Neurosci* 17:5380–5394. <https://doi.org/10.1523/JNEUROSCI.17-14-05380.1997>
- Colino A, Malenka RC (1993) Mechanisms underlying induction of long-term potentiation in rat medial and lateral perforant paths in vitro. *J Neurophysiol* 69:1150–1159
- Deshmukh SS, Knierim JJ (2011) Representation of non-spatial and spatial information in the lateral entorhinal cortex. *Front Behav Neurosci* 5:69. <https://doi.org/10.3389/fnbeh.2011.00069>
- Deshmukh SS, Yoganarasimha D, Voicu H, Knierim JJ (2010) Theta modulation in the medial and the lateral entorhinal cortices. *J Neurophysiol* 104:994–1006. <https://doi.org/10.1152/jn.01141.2009>
- Espinoza C, Guzman SJ, Zhang X, Jonas P (2018) Parvalbumin(+) interneurons obey unique connectivity rules and establish a powerful lateral-inhibition microcircuit in dentate gyrus. *Nat Commun* 9:4605. <https://doi.org/10.1038/s41467-018-06899-3>
- Fernández-Ruiz A, Oliva A, Soula M et al (2021) Gamma rhythm communication between entorhinal cortex and dentate gyrus neuronal assemblies. *Science*. <https://doi.org/10.1126/science.abf3119>
- Ferrante M, Migliore M, Ascoli GA (2009) Feed-forward inhibition as a buffer of the neuronal input-output relation. *Proc Natl Acad Sci U S A* 106:18004–18009. <https://doi.org/10.1073/pnas.0904784106>
- Hayakawa H, Samura T, Kamiyo TC et al (2015) Spatial information enhanced by non-spatial information in hippocampal granule cells. *Cogn Neurodyn* 9:1–12. <https://doi.org/10.1007/s11571-014-9309-x>
- Hines ML, Carnevale NT (1997) The neuron simulation environment. *Neural Comput* 9:1179–1209. <https://doi.org/10.1162/neco.1997.9.6.1179>
- Igarashi J, Hayashi H, Tateno K (2007) Theta phase coding in a network model of the entorhinal cortex layer II with entorhinal-hippocampal loop connections. *Cogn Neurodyn* 1:169–184. <https://doi.org/10.1007/s11571-006-9003-8>
- Igarashi KM, Lu L, Colgin LL et al (2014) Coordination of entorhinal-hippocampal ensemble activity during associative learning. *Nature* 510:143–147. <https://doi.org/10.1038/nature13162>
- Ishizuka S, Nakashima K, Tateno K, Hayashi H (2004) Selective communication and a band-pass filter in the rat dentate gyrus. *Int Congr Ser* 1269:77–80. <https://doi.org/10.1016/j.ics.2004.05.040>
- Jeewajee A, Barry C, O’Keefe J, Burgess N (2008) Grid cells and theta as oscillatory interference: electrophysiological data from freely moving rats. *Hippocampus* 18:1175–1185. <https://doi.org/10.1002/hipo.20510>
- McNaughton BL (1980) Evidence for two physiologically distinct perforant pathways to the fascia dentata. *Brain Res* 199:1–19. [https://doi.org/10.1016/0006-8993\(80\)90226-7](https://doi.org/10.1016/0006-8993(80)90226-7)
- Nishimura-Akiyoshi S, Niimi K, Nakashiba T, Itohara S (2007) Axonal netrin-Gs transneuronally determine lamina-specific subdendritic segments. *Proc Natl Acad Sci U S A* 104:14801–14806. <https://doi.org/10.1073/pnas.0706919104>
- O’Keefe J, Recce ML (1993) Phase relationship between hippocampal place units and the EEG theta rhythm. *Hippocampus* 3:317–330. <https://doi.org/10.1002/hipo.450030307>
- Petersen RP, Moradpour F, Eadie BD et al (2013) Electrophysiological identification of medial and lateral perforant path inputs to the dentate gyrus. *Neuroscience* 252:154–168. <https://doi.org/10.1016/j.neuroscience.2013.07.063>
- Skaggs WE, McNaughton BL, Wilson MA, Barnes CA (1996) Theta phase precession in hippocampal neuronal populations and the compression of temporal sequences. *Hippocampus* 6:149–172. [https://doi.org/10.1002/\(sici\)1098-1063\(1996\)6:2%3c149::AID-HIPO6%3e3.0.CO;2-K](https://doi.org/10.1002/(sici)1098-1063(1996)6:2%3c149::AID-HIPO6%3e3.0.CO;2-K)
- Sullivan D, Mizuseki K, Sorgi A, Buzsáki G (2014) Comparison of sleep spindles and theta oscillations in the hippocampus. *J Neurosci Off J Soc Neurosci* 34:662–674. <https://doi.org/10.1523/JNEUROSCI.0552-13.2014>
- Sun X, Bernstein MJ, Meng M et al (2020) Functionally distinct neuronal ensembles within the memory engram. *Cell* 181:410–423.e17. <https://doi.org/10.1016/j.cell.2020.02.055>

- Tsodyks M, Pawelzik K, Markram H (1998) Neural networks with dynamic synapses. *Neural Comput* 10:821–835. <https://doi.org/10.1162/089976698300017502>
- Tuncdemir SN, Grosmark AD, Turi GF et al (2022) Parallel processing of sensory cue and spatial information in the dentate gyrus. *Cell Rep* 38:110257. <https://doi.org/10.1016/j.celrep.2021.110257>
- Xu W, Wilson DA (2012) Odor-evoked activity in the mouse lateral entorhinal cortex. *Neuroscience* 223:12–20. <https://doi.org/10.1016/j.neuroscience.2012.07.067>
- Young BJ, Otto T, Fox GD, Eichenbaum H (1997) Memory representation within the parahippocampal region. *J Neurosci*

17:5183–5195. <https://doi.org/10.1523/JNEUROSCI.17-13-05183.1997>

**Publisher's Note** Springer Nature remains neutral with regard to jurisdictional claims in published maps and institutional affiliations.

Springer Nature or its licensor (e.g. a society or other partner) holds exclusive rights to this article under a publishing agreement with the author(s) or other rightsholder(s); author self-archiving of the accepted manuscript version of this article is solely governed by the terms of such publishing agreement and applicable law.